

# Superconductivity and crystalline electric field effects in the filled skutterudite series $\text{Pr}(\text{Os}_{1-x}\text{Ru}_x)_4\text{Sb}_{12}$

N. A. Frederick, T. D. Do, P.-C. Ho, N. P. Butch, V. S. Zapf, and M. B. Maple  
*Department of Physics and Institute for Pure and Applied Physical Sciences,*  
*University of California at San Diego, La Jolla, CA*

(Dated: November 2, 2018)

X-ray powder diffraction, magnetic susceptibility  $\chi(T)$ , and electrical resistivity  $\rho(T)$  measurements were made on single crystals of the filled skutterudite series  $\text{Pr}(\text{Os}_{1-x}\text{Ru}_x)_4\text{Sb}_{12}$ . One end of the series ( $x = 0$ ) is a heavy fermion superconductor with a superconducting critical temperature  $T_c = 1.85$  K, while the other end ( $x = 1$ ) is a conventional superconductor with  $T_c \approx 1$  K. The lattice constant  $a$  decreases approximately linearly with increasing Ru concentration  $x$ . As Ru (Os) is substituted for Os (Ru),  $T_c$  decreases nearly linearly with substituent concentration and exhibits a minimum with a value of  $T_c = 0.75$  K at  $x = 0.6$ , suggesting that the two types of superconductivity compete with one another. Crystalline electric field (CEF) effects in  $\chi_{\text{dc}}(T)$  and  $\rho(T)$  due to the splitting of the  $\text{Pr}^{3+}$  nine-fold degenerate Hund's rule  $J = 4$  multiplet are observed throughout the series, with the splitting between the ground state and the first excited state increasing monotonically as  $x$  increases. The fits to the  $\chi_{\text{dc}}(T)$  and  $\rho(T)$  data are consistent with a  $\Gamma_3$  doublet ground state for all values of  $x$ , although reasonable fits can be obtained for a  $\Gamma_1$  ground state for  $x$  values near the end member compounds ( $x = 0$  or  $x = 1$ ).

PACS numbers: 71.27.+a, 74.25.Fy, 74.25.Ha, 74.62.Dh

## I. INTRODUCTION

The filled skutterudite compound  $\text{PrOs}_4\text{Sb}_{12}$  was recently discovered to be the first Pr-based heavy fermion superconductor, with a superconducting transition temperature  $T_c = 1.85$  K and an effective mass  $m^* \approx 50 m_e$ , where  $m_e$  is the free electron mass.<sup>1,2</sup> Features in the dc magnetic susceptibility  $\chi_{\text{dc}}(T)$ , specific heat  $C(T)$ , electrical resistivity  $\rho(T)$ , and inelastic neutron scattering (INS) can be associated with the thermally dependent population of the ninefold degenerate  $\text{Pr}^{3+}$   $J = 4$  Hund's rule multiplet split by a cubic crystalline electric field (CEF). These data suggest that the ground state of  $\text{PrOs}_4\text{Sb}_{12}$  is a  $\Gamma_3$  doublet, separated from a  $\Gamma_5$  triplet first excited state by  $\sim 10$  K.<sup>1,2</sup> The possibility of a  $\Gamma_1$  singlet ground state has also been put forward based on other measurements,<sup>3,4</sup> some of which also consider tetrahedral symmetry operators in their calculations of the CEF Hamiltonian of  $\text{PrOs}_4\text{Sb}_{12}$ .<sup>5</sup> It has been proposed that the superconductivity in  $\text{PrOs}_4\text{Sb}_{12}$  may be due to quadrupolar fluctuations,<sup>1</sup> a claim that has been supported by  $\mu\text{SR}$ <sup>6</sup> and Sb-NQR<sup>7</sup> measurements, which indicate a strong-coupling isotropic energy gap of  $2\Delta \approx 5k_B T_c$ . Other intriguing effects are seen in  $\text{PrOs}_4\text{Sb}_{12}$ , including multiple superconducting transitions<sup>8,9,10</sup> and phases,<sup>11</sup> and an ordered phase that is observed in high magnetic fields and low temperatures.<sup>12</sup> This high field ordered phase (HFOP), which is seen in measurements of  $\rho(T)$ ,<sup>12</sup>  $C(T)$ ,<sup>3,9</sup> magnetization  $M(T)$ ,<sup>13</sup> thermal expansion  $\alpha(T)$ ,<sup>10</sup> and magnetostriction  $\lambda(T)$ <sup>14</sup> in a magnetic field  $H$ , as well as measurements of  $\rho(H)$  isotherms,<sup>13</sup> appears to be related to the crossing of the CEF energy levels in magnetic fields.<sup>9,15</sup> In addition, neutron diffraction experiments<sup>4</sup> indicate the presence of quadrupolar effects in the HFOP, analogous to those seen in  $\text{PrPb}_3$ .<sup>16</sup>

$\text{PrOs}_4\text{Sb}_{12}$  has proven to be a unique compound, and will continue to provide a fertile area of research for many years.

The isostructural compound  $\text{PrRu}_4\text{Sb}_{12}$  displays superconductivity below  $T_c \approx 1.0$  K and possesses an electronic specific heat coefficient  $\gamma$  approximately 5 to 10 times smaller than  $\text{PrOs}_4\text{Sb}_{12}$ , identifying it as a conventional metal, or at most a borderline heavy fermion metal.<sup>17</sup> It was previously reported, based on measurements of  $\chi_{\text{dc}}(T)$ , to possess a  $\Gamma_1$  ground state and a  $\Gamma_4$  triplet first excited state  $\approx 70$  K above the ground state.<sup>17</sup> A later measurement of  $\rho(T)$  also supported this CEF level scheme.<sup>18</sup>  $\text{PrRu}_4\text{Sb}_{12}$  appears to be a BCS-like weak-coupling superconductor, with an isotropic s-wave energy gap of  $2\Delta \approx 3k_B T_c$ , as determined from Sb-NQR measurements.<sup>19</sup> At the present time, no quadrupolar effects or features resembling the HFOP seen in  $\text{PrOs}_4\text{Sb}_{12}$  have been reported in  $\text{PrRu}_4\text{Sb}_{12}$ .

The substitution of  $\text{PrRu}_4\text{Sb}_{12}$  into  $\text{PrOs}_4\text{Sb}_{12}$  to form  $\text{Pr}(\text{Os}_{1-x}\text{Ru}_x)_4\text{Sb}_{12}$  was undertaken to investigate the evolution of the superconductivity, the CEF energy level scheme, and the heavy fermion state with Ru-doping, and to investigate the relationship, if any, between these three phenomena. The present study focuses on measurements of  $\chi(x, T)$  and  $\rho(x, T)$ , which have revealed the  $x$ -dependencies of  $T_c$  and the splitting between the CEF ground state and the first excited state. We are also in the process of investigating the heavy fermion state via measurements of  $C(T)$ , and the upper critical field  $H_{c2}(T)$  through measurements of  $\rho(T, H)$  (which will also reveal the  $x$ -dependence of the HFOP), and will report these results in a future publication.

## II. EXPERIMENTAL DETAILS

Single crystals of  $\text{Pr}(\text{Os}_{1-x}\text{Ru}_x)_4\text{Sb}_{12}$  were grown using an Sb flux method. The elements (Ames 5N Pr, Colonial Metals 3.5N Os and 3N Ru, and Alfa Aesar 6N Sb) were sealed under 150 Torr Ar in a carbon-coated quartz tube in the ratio 1 : 4 - 4x : 4x : 20, heated to 1050 °C at 50 °C/hr, then cooled at 2 °C/hr to 700 °C. The samples were then removed from the furnace and the excess Sb was spun off in a centrifuge. The crystals were removed from the leftover flux by etching with dilute Aqua Regia ( $\text{HCl}:\text{HNO}_3:\text{H}_2\text{O} = 1 : 1 : 3$ ).

X-ray powder diffraction measurements were made at room temperature using a Rigaku D/MAX B x-ray machine. The only significant impurities in any of the samples were identified with free Sb that was still attached to the crystals. Each  $\text{Pr}(\text{Os}_{1-x}\text{Ru}_x)_4\text{Sb}_{12}$  sample crystallized in the  $\text{LaFe}_4\text{P}_{12}$  structure<sup>20</sup> with a lattice constant  $a$  that decreased roughly linearly with increasing Ru concentration  $x$ , as displayed in Fig. 1. A silicon standard was used in order to achieve a more accurate determination of the lattice constant. Measurements of  $\chi_{\text{dc}}$  vs temperature  $T$  were made in a magnetic field  $H$  of 0.5 tesla between 1.8 and 300 K in a commercial Quantum Design superconducting quantum interference device (SQUID) magnetometer. Measurements of  $\rho$  and  $\chi_{\text{ac}}$  were made as a function of  $T$  down to 1.2 K in a  $^4\text{He}$  cryostat and, for several of the samples, down to 0.1 K in a  $^3\text{He}$ - $^4\text{He}$  dilution refrigerator.

## III. RESULTS

### A. Magnetic Susceptibility

Displayed in the main portion of Fig. 2 is a plot of the dc magnetic susceptibility  $\chi_{\text{dc}}$  as a function of temperature  $T$  for single crystals of  $\text{Pr}(\text{Os}_{1-x}\text{Ru}_x)_4\text{Sb}_{12}$  with various values of  $x$ . Above  $T \approx 100$  K, the inverse magnetic susceptibility  $1/\chi_{\text{dc}}$  is linear, indicating Curie-Weiss behavior. The data have been corrected for excess Sb by assuming that the high temperature effective moment,  $\mu_{\text{eff}}$ , of Pr should be equal to the Hund's rule free ion value of  $3.58 \mu_B$  for  $\text{Pr}^{3+}$ , where  $\mu_B$  is the Bohr magneton. Any deviation from this value was attributed to free Sb inclusions in the  $\text{Pr}(\text{Os}_{1-x}\text{Ru}_x)_4\text{Sb}_{12}$  crystals. The most significant effect on  $\chi_{\text{dc}}$  from this correction was not the small diamagnetic Sb signal but instead the change in overall scaling due to the difference in mass used to calculate  $\chi_{\text{dc}}$  in units of  $\text{cm}^3/\text{mol}$  from the raw magnetization data. The calculated percentages of mass attributed to Sb out of the total sample volume for all values of  $x$  are listed in Table I. The estimated value of the Sb mass depends slightly on the CEF ground state used to make the fit correction; only the values for a  $\Gamma_3$  ground state are given for simplicity.

All of the  $\text{Pr}(\text{Os}_{1-x}\text{Ru}_x)_4\text{Sb}_{12}$  samples exhibit features (peaks or plateaus) in  $\chi_{\text{dc}}$  that can be attributed to CEF

effects. These features are the focus of the two insets in Fig. 2. The low temperature  $\chi_{\text{dc}}$  data for the samples from  $x = 0$  to  $x = 0.4$  are shown in Fig. 2(a), while Fig. 2(b) similarly displays data for the samples from  $x = 0.5$  to  $x = 1$ . An explanation of the fits used to determine the CEF parameters from the  $\chi_{\text{dc}}$  data, as well as the parameters themselves, is given in section IV B.

Low temperature ( $< 2$  K) ac magnetic susceptibility  $\chi_{\text{ac}}$  vs  $T$  data for  $\text{Pr}(\text{Os}_{1-x}\text{Ru}_x)_4\text{Sb}_{12}$  are shown in Fig. 3. A sharp diamagnetic transition can be seen for all values of  $x$ , indicating the presence of superconductivity. The superconducting critical temperature  $T_c$  for each concentration was determined from the data displayed in Fig. 3 as the midpoint of the diamagnetic transition. A plot of  $T_c$  vs  $x$  is displayed in Fig. 6, and is discussed further in section IV A. An additional feature of note is the step-like structure that appears in the  $\chi_{\text{ac}}$  data for  $\text{PrOs}_4\text{Sb}_{12}$ . Since double superconducting transitions have been observed in specific heat and thermal expansion measurements on both collections of single crystals and individual single crystals,<sup>8,9,10</sup> it is reasonable to assume that this step in the diamagnetic transition for  $\text{PrOs}_4\text{Sb}_{12}$  is also due to an intrinsic second superconducting phase instead of a variation of  $T_c$  throughout the multiple crystals used in the  $\chi_{\text{ac}}$  measurements. None of the other concentrations display significant structure in their superconducting transitions, although the transitions for  $x = 0.3$  and  $x = 0.4$  are much wider than for the other concentrations. This may be due to a variation of  $T_c$  between individual crystals for these two concentrations.

### B. Electrical Resistivity

Fig. 4 displays high-temperature electrical resistivity  $\rho$  vs  $T$  data for  $\text{Pr}(\text{Os}_{1-x}\text{Ru}_x)_4\text{Sb}_{12}$  for various values of  $x$  between 0 and 1. The values of  $\rho$  at room temperature,  $\rho(300 \text{ K})$ , and the extrapolated values of  $\rho$  at zero temperature from fits to the  $\rho(T)$  data based on calculations of  $\rho(T)$  that incorporate CEF splitting of the  $\text{Pr}^{3+}$   $J = 4$  multiplet (see section IV B),  $\rho(0 \text{ K})$ , are listed in Table I. Also listed in Table I is the residual resistivity ratio (RRR), defined as  $\rho(300 \text{ K})/\rho(0 \text{ K})$ . It is surprising that the RRR of  $\text{PrRu}_4\text{Sb}_{12}$  is so much lower than that of  $\text{PrOs}_4\text{Sb}_{12}$ , since they are both stoichiometric compounds and would be expected to have a low residual resistivity. A previous measurement of  $\text{PrRu}_4\text{Sb}_{12}$  found  $\rho(300 \text{ K}) = 632 \mu\Omega \text{ cm}$  and an RRR of 25,<sup>17</sup> in reasonable agreement with the data presented in this paper. The low RRR of  $\text{PrRu}_4\text{Sb}_{12}$  is not presently understood.

The electrical resistivity of  $\text{Pr}(\text{Os}_{1-x}\text{Ru}_x)_4\text{Sb}_{12}$  below  $T = 2 \text{ K}$  is shown in Fig. 5. The data have been normalized to their values at 2 K in order to emphasize the superconducting transitions. The  $x = 0.7$  sample did not display the onset of superconductivity down to the lowest measured temperatures and no data for this sample are shown in this plot; the heating due to large contact resistances in the  $x = 0.7$  and  $x = 0.9$  samples precluded

measurements below 1 K. The superconducting transitions as determined from  $\rho(T)$  are in reasonable agreement with those measured inductively (Fig. 3), and the plot of  $T_c$  vs  $x$  is discussed in the following section.

## IV. ANALYSIS AND DISCUSSION

### A. Superconductivity

The dependence of the superconducting transition temperature  $T_c$  on Ru concentration  $x$  for  $\text{Pr}(\text{Os}_{1-x}\text{Ru}_x)_4\text{Sb}_{12}$  is shown in Fig. 6. Several concentrations have more than one data point associated with them, which are from measurements of different crystals. These additional measurements were not shown in Figs. 4 and 5 or listed in Table I in the interest of clarity. The RRRs were nearly identical for all crystals of a given concentration, with the exception of the  $x = 0.2$  samples where the crystal with the lowest  $T_c$  in Fig. 6 had an RRR about half of that measured for the other two  $x = 0.2$  samples, one of which is listed in Table I. The vertical bars in Fig. 6 are a measure of the width of the superconducting transitions, taken to be the 10% and 90% values of the resistance change associated with the transition.

The trend of the  $T_c$  vs  $x$  data shown in Fig. 6 suggests a competition between the two different types of superconductivity seen in  $\text{PrOs}_4\text{Sb}_{12}$  and  $\text{PrRu}_4\text{Sb}_{12}$ . This competition suppresses  $T_c$  from both ends, culminating in a minimum of  $T_c = 0.75$  K near  $x = 0.6$ . Specific heat measurements are in progress, and it will be interesting to see if the heavy fermion state can be correlated with  $T_c$ . The persistence of superconductivity throughout the series is unusual, as for heavy fermion f-electron superconductors both magnetic and nonmagnetic impurities generally produce relatively rapid depressions of  $T_c$ . When the impurity is of an element that would produce an isostructural superconducting compound, the trend is not as clear. For example, the  $\text{U}_{1-x}\text{La}_x\text{Pd}_2\text{Al}_3$  system is similar to the  $\text{Pr}(\text{Os}_{1-x}\text{Ru}_x)_4\text{Sb}_{12}$  system in that one end member compound,  $\text{UPd}_2\text{Al}_3$ , is a heavy fermion superconductor, while the other end member compound,  $\text{LaPd}_2\text{Al}_3$ , is a conventional BCS superconductor. Unlike  $\text{Pr}(\text{Os}_{1-x}\text{Ru}_x)_4\text{Sb}_{12}$ , however, superconductivity is destroyed upon substitution on either end of the series.<sup>21</sup> This persistence of superconductivity throughout of the  $\text{Pr}(\text{Os}_{1-x}\text{Ru}_x)_4\text{Sb}_{12}$  system for all values of  $x$  is observed in the  $\text{CeCo}_{1-x}\text{Ir}_x\text{In}_5$  series of compounds, which is also superconducting for all values of  $x$ .<sup>22</sup> This system's similarities to  $\text{Pr}(\text{Os}_{1-x}\text{Ru}_x)_4\text{Sb}_{12}$  end there, because both end member compounds ( $\text{CeCoIn}_5$  and  $\text{CeIrIn}_5$ ) are heavy fermion superconductors in which the superconductivity is believed to be magnetically mediated and to possess nodes in the energy gap  $\Delta(\mathbf{k})$ .<sup>23</sup>

This nodal energy gap structure may be in contrast with  $\text{PrOs}_4\text{Sb}_{12}$ , where  $\mu\text{SR}$ <sup>6</sup> and  $\text{Sb-NQR}$ <sup>7</sup> measurements indicate an isotropic energy gap, a condition which

could occur if the superconductivity in  $\text{PrOs}_4\text{Sb}_{12}$  was mediated by quadrupolar fluctuations. It is also generally the case that superconductors with isotropic or nearly isotropic energy gaps are relatively insensitive to the presence of nonmagnetic impurities. Thus, the gradual decrease of  $T_c$ , and the presence of superconductivity for all values of  $x$  in  $\text{Pr}(\text{Os}_{1-x}\text{Ru}_x)_4\text{Sb}_{12}$ , provides further evidence for an isotropic energy gap and quadrupolar superconductivity in  $\text{PrOs}_4\text{Sb}_{12}$ , since  $\text{PrRu}_4\text{Sb}_{12}$  also possesses an isotropic superconducting energy gap.<sup>19</sup> The minimum in  $T_c$  near  $x = 0.6$  could then be attributed to a shift from quadrupolar mediated heavy fermion superconductivity to phonon mediated BCS superconductivity. On the other hand, thermal conductivity measurements of  $\text{PrOs}_4\text{Sb}_{12}$  in a magnetic field have been interpreted in terms of two distinct superconducting phases in the  $H - T$  plane, one with two point nodes in  $\Delta(\mathbf{k})$  in low fields, and another with six point nodes in  $\Delta(\mathbf{k})$  at higher fields.<sup>11</sup> Since no thermal conductivity measurements were reported for fields below 0.3 T, the structure of  $\Delta(\mathbf{k})$  is not known below this field. It is conceivable that, just as a magnetic field induces a change from a state with two point nodes into a state with six point nodes, the state with two point nodes is itself induced from an isotropic zero-field energy gap. Further measurements of the energy gap symmetry in zero and low magnetic field could shed light on this mystery.

### B. Crystalline Electric Field Effects

The  $\chi_{\text{dc}}(T)$  and  $\rho(T)$  data for  $\text{Pr}(\text{Os}_{1-x}\text{Ru}_x)_4\text{Sb}_{12}$  were fit to equations including CEF effects, in a manner identical to that reported previously.<sup>1,15</sup> The CEF equations were derived from the Hamiltonian of Lea, Leask and Wolf (LLW).<sup>24</sup> In the LLW formalism, the CEF energy levels are given in terms of the parameters  $x_{\text{LLW}}$  and  $W$ , where  $x_{\text{LLW}}$  is the ratio of the fourth and sixth order terms of the angular momentum operators and  $W$  is an overall energy scale factor. It was assumed that the CEF parameter  $y$  which controls the tetrahedral  $T_h$  crystalline symmetry contribution to the Hamiltonian<sup>5</sup> was small; thus, the calculations were made for a cubic  $O_h$  crystalline symmetry. Assuming that  $y$  is small implies that the main contribution to the crystalline electric field comes from the simple cubic transition metal sublattice (Os or Ru), as opposed to the more complicated tetrahedral Sb sublattice. The  $\chi_{\text{dc}}(T)$  data for  $x \leq 0.15$  could be reasonably fit with either a  $\Gamma_3$  or a  $\Gamma_1$  ground state and a  $\Gamma_5$  first excited state. As  $x$  increases, the magnitude of the peak in  $\chi_{\text{dc}}$  decreases more rapidly than the temperature  $T_{\text{max}}$  at which the peak occurs. The peak also broadens until it resembles a hump. These changes with  $x$  make it unreasonable to fit a  $\Gamma_1$ - $\Gamma_5$  CEF energy level scheme to the higher  $x$  data, since for these data an energy level scheme with the correct  $T_{\text{max}}$  makes the peak too sharp, while the correct hump shape results in a  $T_{\text{max}}$  that is too high. Thus, for the  $\text{Pr}(\text{Os}_{1-x}\text{Ru}_x)_4\text{Sb}_{12}$

samples with  $x \geq 0.2$ , a  $\Gamma_3$  ground state best approximated the data. An example of a fit with a  $\Gamma_3$  ground state for  $x = 0.6$  is shown in Fig. 7(a). A plot of the splitting between the ground state and the first excited state vs  $x$  is shown in Fig. 8, including all reasonable fits of the  $\chi_{dc}(T)$  data.

The  $\text{Pr}(\text{Os}_{1-x}\text{Ru}_x)_4\text{Sb}_{12}$  samples with  $x \geq 0.6$  all display upturns in  $\chi_{dc}(T)$  at the lowest temperatures (inset (b) in Fig. 2). If these upturns are due to the splitting of the CEF energy levels in a small magnetic field  $H$ , then it is expected that they would be more visible in the samples with large  $x$  (more Ru than Os), where  $\chi_{dc}$  is smaller at low temperatures compared to the small  $x$  (more Os than Ru) data. The samples with  $x \geq 0.75$ , including  $\text{PrRu}_4\text{Sb}_{12}$ , also display structure in these upturns that appear to be an additional peak near 5 K superimposed on the broad CEF hump, near the temperature of the CEF peak in  $\text{PrOs}_4\text{Sb}_{12}$ . The smooth progression of both the lattice parameter  $a$  and  $T_c$  indicates that there is no macroscopic phase separation of  $\text{Pr}(\text{Os}_{1-x}\text{Ru}_x)_4\text{Sb}_{12}$  into  $\text{PrOs}_4\text{Sb}_{12}$  and  $\text{PrRu}_4\text{Sb}_{12}$ . However, it is possible that the peak-like structure could be due to inhomogeneous alloying of Os and Ru on an atomic scale, wherein each  $\text{Pr}^{3+}$  ion sees a distribution of Os or Ru atoms, leading to a variation in the CEF throughout the crystal. Unfortunately, this possibility would be difficult to establish in the current experiments. The low-temperature upturn, especially in  $\text{PrRu}_4\text{Sb}_{12}$ , could be attributed to either CEF splitting in  $H$  or paramagnetic impurities, both of which could produce a low-temperature increase in  $\chi_{dc}$ .

Takeda et al. reported that  $\text{PrRu}_4\text{Sb}_{12}$  had a  $\Gamma_1$  singlet ground state and a  $\Gamma_4$  triplet first excited state, a CEF configuration that exhibits a plateau in  $\chi_{dc}$  at low temperatures.<sup>17</sup> In the current experiment, the  $x = 0.9$  and  $x = 1$  samples are the only ones in which a plateau is observed. In addition, while the other samples with  $x \geq 0.85$  have their peaks reasonably well described by a  $\Gamma_3$  ground state, the fit predicts a saturation at  $T = 0$  K that is much lower than is observed in the data. However, the low- $T$  upturn could be responsible for disguising both the maximum in  $x = 0.9$  and  $x = 1$  and the low temperature saturation observed in the other high Ru concentration samples. Accordingly, all the  $\text{Pr}(\text{Os}_{1-x}\text{Ru}_x)_4\text{Sb}_{12}$  data with  $x \geq 0.85$  were fit assuming both a  $\Gamma_3 - \Gamma_5$  CEF energy level scheme and a  $\Gamma_1 - \Gamma_4$  scheme, ignoring the low-temperature upturn; the  $x = 0.85$  fits are shown in Fig. 7(b). Both fits are represented in the splitting between the ground state and first excited state  $\Delta E_{gs-1es}$  vs  $x$  plot of Fig. 8; the results from all fits are also listed in Table I.

The electrical resistivity  $\rho(T)$  of  $\text{Pr}(\text{Os}_{1-x}\text{Ru}_x)_4\text{Sb}_{12}$  was fit by a combination of scattering from impurities, the atomic lattice (phonons), and temperature-dependent energy level populations due to the CEF.<sup>15</sup> The phonon contribution was represented by the measured  $\rho_{\text{lat}}$  of  $\text{LaOs}_4\text{Sb}_{12}$ , an isostructural reference compound without f-electrons, for all values of  $x$ . This pro-

cedure was validated by reproducing the results of Abe et al.<sup>18</sup> with  $\text{LaOs}_4\text{Sb}_{12}$  instead of  $\text{LaRu}_4\text{Sb}_{12}$ ; as expected, the  $\rho_{\text{lat}}$  data of the two compounds appear to be nearly identical. The CEF contribution to  $\rho(T)$  consists of two terms, representing magnetic exchange and aspherical Coulomb scattering, which were assumed to be equally important when fitting the data.<sup>15</sup> Just as it was possible to fit  $\rho(T)$  of  $\text{PrOs}_4\text{Sb}_{12}$  with either a  $\Gamma_3$  or a  $\Gamma_1$  ground state, all of the  $\text{Pr}(\text{Os}_{1-x}\text{Ru}_x)_4\text{Sb}_{12}$  data were indifferent to the choice of either ground state. The splitting between the ground state and the first excited state (always a  $\Gamma_5$  triplet) was also nearly identical for fits with either ground state for a particular value of  $x$ . In the interest of simplicity, for the  $\rho(T)$  data, only the splitting between  $\Gamma_3$  and  $\Gamma_5$ ,  $\Delta E_{3-5}$ , is shown in Fig. 8. The fit used to calculate  $\Delta E_{3-5}$  for  $x = 0.15$  is shown in Fig. 7(b). It is evident that  $\rho(H)$  measurements will be required to elucidate the CEF ground state from transport measurements.<sup>15</sup>

It is unclear what effect the CEF ground state may have on the superconductivity in  $\text{Pr}(\text{Os}_{1-x}\text{Ru}_x)_4\text{Sb}_{12}$ . From a physical point of view, it is reasonable that an abrupt change in the ground state would produce an equally abrupt change in the physical properties. However, it is difficult to conceive of a mechanism for this occurrence in the context of the LLW theory, since it is based on the interaction of the atomic lattice with a rare earth ion. If there is not an abrupt change in the lattice structure, one should not expect an abrupt change in the CEF ground state. It is therefore far more reasonable to consider a constant ground state, with the excited state varying as the Ru substitution changes the spacing of the atoms in the skutterudite lattice. The present data are most consistent with a constant  $\Gamma_3$  ground state, with the exception of the  $x = 0.9$  and  $x = 1$  data. However, when  $x$  is in the region  $0.2 \leq x \leq 0.75$  a  $\Gamma_3 - \Gamma_5$  CEF energy level scheme is the only one which reasonably fits the  $\chi_{dc}(T, x)$  data. On the other hand, the possibility cannot be ruled out that this deep in a substituted system, a CEF analysis in the tradition of LLW may be unreliable due to the distribution of the two substituents (Os and Ru) in the near neighbor environment of each  $\text{Pr}^{3+}$  ion. The gradual metamorphosis of the  $\chi_{dc}$  data does suggest that the CEF parameters are also changing gradually, but this may be misleading. Further experiments as well as theoretical analysis will be necessary to completely reveal the CEF ground state and its relationship to the superconductivity.

## V. SUMMARY

The superconducting critical temperature  $T_c$  and crystalline electric field (CEF) parameters of single crystals of  $\text{Pr}(\text{Os}_{1-x}\text{Ru}_x)_4\text{Sb}_{12}$  have been deduced through measurements of  $\chi(T)$  and  $\rho(T)$  for  $0 \leq x \leq 1$ . The superconductivity, which is present for all values of  $x$ , exhibits a change in the sign of the slope in  $T_c(x)$  near

$x = 0.6$ . The CEF ground state may also change from a  $\Gamma_3$  ground state to a  $\Gamma_1$  ground state near this concentration, although more measurements are necessary to confirm this possibility. It is possible that the crossover from heavy fermion superconductivity that may be mediated by quadrupolar interactions to nearly BCS superconductivity occurs at this ‘pseudocritical’ concentration  $x_{pc} = 0.6$ .

### Acknowledgements

We would like to thank S. K. Kim and D. T. Walker for experimental assistance, and E. D. Bauer for useful

discussions. This research was supported by the U.S. Department of Energy Grant No. DE-FG03-86ER-45230, the U.S. National Science Foundation Grant No. DMR-00-72125, and the NEDO International Joint Research Program.

- 
- <sup>1</sup> E. D. Bauer, N. A. Frederick, P.-C. Ho, V. S. Zapf, and M. B. Maple, *Phys. Rev. B* **65**, 100506(R) (2002).
  - <sup>2</sup> M. B. Maple, P.-C. Ho, V. S. Zapf, N. A. Frederick, E. D. Bauer, W. M. Yuhasz, F. M. Woodward, and J. W. Lynn, *J. Phys. Soc. Jpn.* **71** **Suppl.**, 23 (2002).
  - <sup>3</sup> Y. Aoki, T. Namiki, S. Ohsaki, S. R. Saha, H. Sugawara, and H. Sato, *J. Phys. Soc. Jpn.* **71**, 2098 (2002).
  - <sup>4</sup> M. Kohgi, M. Iwasa, M. Nakajima, N. Metoki, S. Araki, N. Bernhoeft, J.-M. Mignot, A. Gukasov, H. Sato, Y. Aoki, and H. Sugawara (unpublished).
  - <sup>5</sup> K. Takegahara, H. Harima, and A. Yanase, *J. Phys. Soc. Jpn.* **70**, 1190 (2001).
  - <sup>6</sup> D. E. MacLaughlin, J. E. Sonier, R. H. Heffner, O. O. Bernal, B.-L. Young, M. S. Rose, G. D. Morris, E. D. Bauer, T. D. Do, and M. B. Maple, *Phys. Rev. Lett.* **89**, 157001 (2002).
  - <sup>7</sup> H. Kotegawa, M. Yogi, Y. Imamura, Y. Kawasaki, G. q. Zheng, Y. Kitaoka, S. Ohsaki, H. Sugawara, Y. Aoki, and H. Sato, *Phys. Rev. Lett.* **90**, 027001 (2003).
  - <sup>8</sup> M. B. Maple, P.-C. Ho, N. A. Frederick, V. S. Zapf, W. M. Yuhasz, and E. D. Bauer, *Acta Physica Polonica B* **34**, 919 (2003).
  - <sup>9</sup> R. Vollmer, A. Faißt, C. Pfeiderer, H. v. Löhneysen, E. D. Bauer, P.-C. Ho, V. S. Zapf, and M. B. Maple, *Phys. Rev. Lett.* **90**, 057001 (2003).
  - <sup>10</sup> N. Oeschler, P. Gegenwart, F. Steglich, N. A. Frederick, E. D. Bauer, and M. B. Maple, *Acta Physica Polonica B* **34**, 959 (2003).
  - <sup>11</sup> K. Izawa, Y. Nakajima, J. Goryo, Y. Matsuda, S. Osaki, H. Sugawara, H. Sato, P. Thalmeier, and K. Maki, *Phys. Rev. Lett.* **90**, 117001 (2003).
  - <sup>12</sup> P.-C. Ho, V. S. Zapf, E. D. Bauer, N. A. Frederick, and M. B. Maple, *Int. J. Mod. Phys. B* **16**, 3008 (2002).
  - <sup>13</sup> P.-C. Ho, N. A. Frederick, V. S. Zapf, E. D. Bauer, T. D. Do, M. B. Maple, A. D. Christianson, and A. H. Lacerda, *Phys. Rev. B* **67**, 180508(R) (2003).
  - <sup>14</sup> N. Oeschler, F. Weickert, P. Gegenwart, P. Thalmeier, F. Steglich, E. D. Bauer, and M. B. Maple, *Phys. Rev. B* (2003), submitted.
  - <sup>15</sup> N. A. Frederick and M. B. Maple, *J. Phys.: Condens. Matter* **15**, 4789 (2003).
  - <sup>16</sup> T. Tayama, T. Sakakibara, K. Kitami, M. Yokoyama, K. Tenya, H. Amitsuka, D. Aoki, Y. Onuki, and Z. Kletowski, *J. Phys. Soc. Jpn.* **70**, 248 (2001).
  - <sup>17</sup> N. Takeda and M. Ishikawa, *J. Phys. Soc. Jpn.* **69**, 868 (2000).
  - <sup>18</sup> K. Abe, H. Sato, T. D. Matsuda, T. Namiki, H. Sugawara, and Y. Aoki, *J. Phys.: Condens. Matter* **14**, 11757 (2002).
  - <sup>19</sup> M. Yogi, H. Kotegawa, Y. Imamura, G. q. Zheng, Y. Kitaoka, H. Sugawara, and H. Sato, *cond-mat/0303569*, (2003).
  - <sup>20</sup> D. J. Braun and W. Jeitschko, *J. Less-Common Met.* **72**, 147 (1980).
  - <sup>21</sup> V. S. Zapf, R. P. Dickey, E. J. Freeman, C. Sirvent, and M. B. Maple, *Phys. Rev. B* **65**, 024437 (2001).
  - <sup>22</sup> P. G. Pagliuso, R. Movshovich, A. D. Bianchi, M. Nicklas, N. O. Moreno, J. D. Thompson, M. F. Hundley, J. L. Sarrao, and Z. Fisk, *Physica B* **312-313**, 129 (2002).
  - <sup>23</sup> R. Movshovich, A. Bianchi, M. Jaime, M. F. Hundley, J. D. Thompson, N. Curro, P. C. Hammel, Z. Fisk, P. G. Pagliuso, and J. L. Sarrao, *Physica B* **312-313**, 7 (2002).
  - <sup>24</sup> K. R. Lea, M. J. M. Leask, and W. P. Wolf, *J. Phys. Chem. Solids* **23**, 1381 (1962).

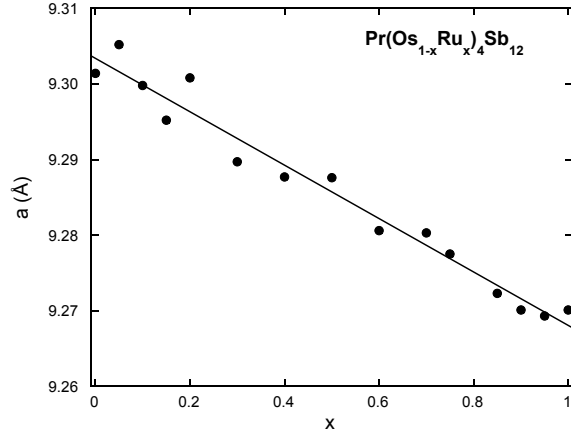


FIG. 1: Lattice parameter  $a$  as a function of Ru concentration  $x$ . The solid line is a linear least squares fit to  $a$  vs  $x$ .

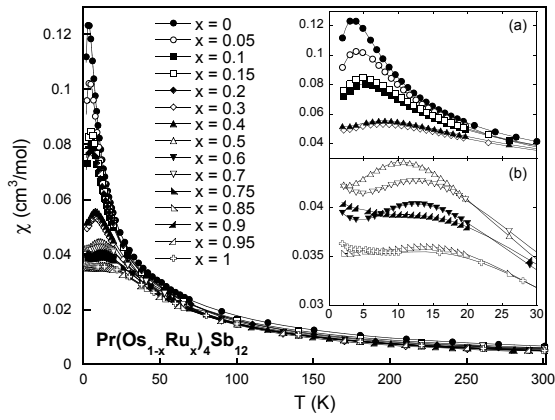


FIG. 2: dc magnetic susceptibility  $\chi_{\text{dc}}$  as a function of temperature  $T$  between 1.8 and 300 K for single crystals of  $\text{Pr}(\text{Os}_{1-x}\text{Ru}_x)_4\text{Sb}_{12}$ . Inset (a):  $\chi_{\text{dc}}$  vs  $T$  between 1.8 and 30 K, showing the evolution of the peak due to crystalline electric field effects for the Ru concentrations  $x = 0$  to  $x = 0.4$ . The  $x = 0.2$  sample has been removed for clarity. Inset (b): as inset (a), but for Ru concentrations  $x = 0.5$  to  $x = 1$ . The samples with  $x = 0.75$  and  $x = 0.95$  were removed for clarity.

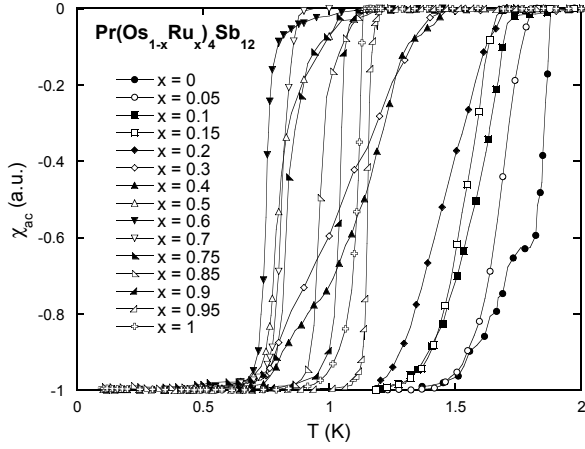


FIG. 3: ac magnetic susceptibility  $\chi_{ac}$  as a function of temperature  $T$  between 0.1 and 2 K for single crystals of  $\text{Pr}(\text{Os}_{1-x}\text{Ru}_x)_4\text{Sb}_{12}$ . The data have been normalized to 0 at  $T = 2$  K and to  $-1$  at  $T = 0$  K for clarity.

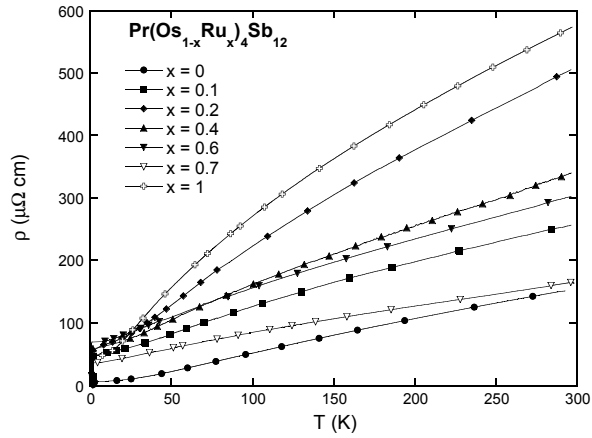


FIG. 4: Electrical resistivity  $\rho$  as a function of temperature  $T$  between 0.4 and 300 K for single crystals of  $\text{Pr}(\text{Os}_{1-x}\text{Ru}_x)_4\text{Sb}_{12}$  with various values of  $x$  between 0 and 1. The samples with  $x = 0.05$ ,  $x = 0.15$ , and  $x = 0.9$  were removed for clarity.

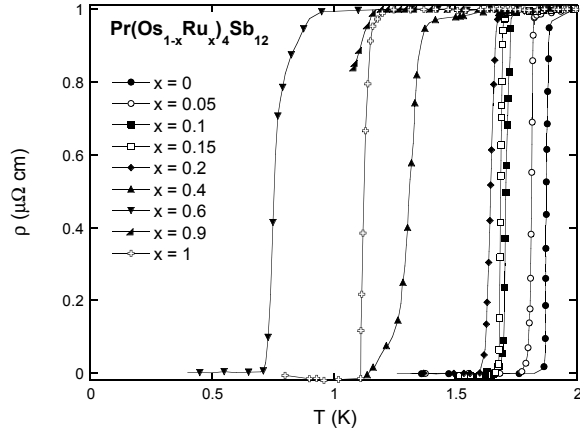


FIG. 5: Electrical resistivity  $\rho$  as a function of temperature  $T$  between 0.4 and 2 K for single crystals of  $\text{Pr}(\text{Os}_{1-x}\text{Ru}_x)_4\text{Sb}_{12}$  with various values of  $x$  between 0 and 1, normalized to their values at 2 K. The data for the sample with  $x = 0.7$  is not shown because it did not superconduct down to the lowest temperature measured (see text for details). Similarly, the superconducting transition for  $x = 0.9$  is not complete due to the limits of the experiment.

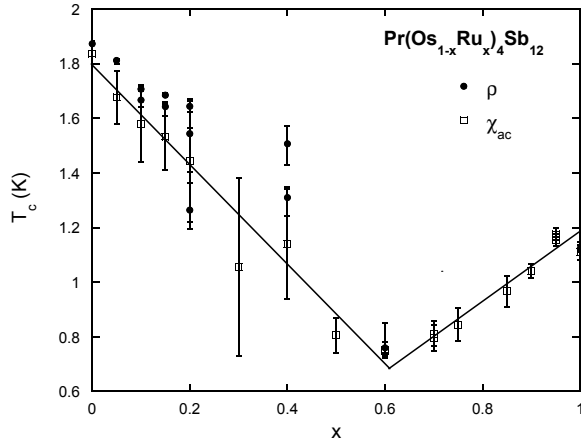


FIG. 6: Superconducting critical temperature  $T_c$  vs Ru concentration  $x$  for  $\text{Pr}(\text{Os}_{1-x}\text{Ru}_x)_4\text{Sb}_{12}$ . Filled circles:  $T_c$  extracted from electrical resistivity  $\rho$ . Open squares:  $T_c$  determined from ac magnetic susceptibility  $\chi_{ac}$ . The straight lines are guides to the eye.



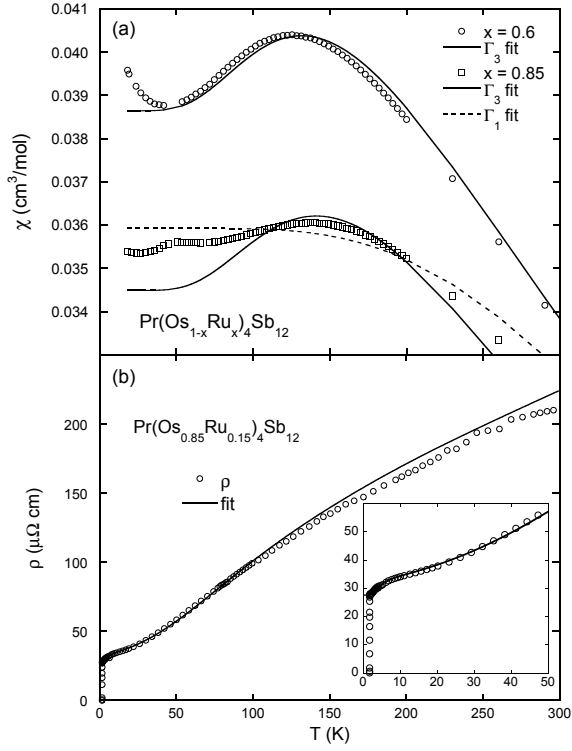


FIG. 7: Examples of CEF fits to the data. (a): dc magnetic susceptibility  $\chi_{\text{dc}}(T)$  for  $x = 0.6$  and  $x = 0.85$  for  $\text{Pr}(\text{Os}_{1-x}\text{Ru}_x)_4\text{Sb}_{12}$ . The solid lines are fits assuming a  $\Gamma_3$  doublet ground state and a  $\Gamma_5$  triplet first excited state, and the dashed line is a fit assuming a  $\Gamma_1$  singlet ground state and a  $\Gamma_4$  triplet first excited state. (b): electrical resistivity  $\rho(T)$  for  $x = 0.15$  between 1 K and 300 K. The fit is for a  $\Gamma_3$  ground state and a  $\Gamma_5$  first excited state. Fits with a  $\Gamma_1$  ground state were qualitatively identical, and so are not shown (see text for details). Inset to (b):  $\rho(T)$  for  $x = 0.15$  between 1 K and 50 K, displaying the low-temperature curvature in greater detail.

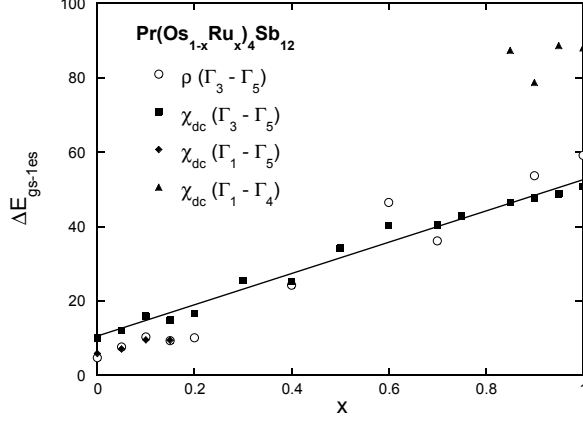


FIG. 8: The splitting between the ground state and first excited state  $\Delta E_{gs-1es}$  vs Ru concentration  $x$  for  $\text{Pr}(\text{Os}_{1-x}\text{Ru}_x)_4\text{Sb}_{12}$ , calculated from fits of CEF equations to  $\chi_{dc}(T)$  and  $\rho(T)$ , as described in the text. The solid line is a linear fit to  $\Delta E_{gs-1es}$  for a  $\Gamma_3$  doublet ground state and a  $\Gamma_5$  triplet first excited state calculated from the  $\chi_{dc}(T)$  data. For  $x \leq 0.15$ , a CEF energy level scheme with a  $\Gamma_1$  singlet ground state and a  $\Gamma_5$  first excited state also provided a reasonable fit to the  $\chi_{dc}(T)$  data, while a  $\Gamma_1$  ground state with a  $\Gamma_4$  triplet first excited state was also a possible energy level scheme for  $x \geq 0.85$ .

TABLE I: Physical properties of  $\text{Pr}(\text{Os}_{1-x}\text{Ru}_x)_4\text{Sb}_{12}$  compounds.  $x$  is the concentration of Ru;  $\rho(300\text{ K})$  is the electrical resistivity  $\rho$  at 300 K;  $\rho(0\text{ K})$  is  $\rho$  at 0 K extrapolated from CEF fits (see text); RRR is the residual resistivity ratio, defined as  $\rho(300\text{ K})/\rho(0\text{ K})$ ; %Sb is the percentage of the mass attributed to free Sb in  $\chi_{dc}(T)$  assuming a  $\Gamma_3$  ground state;  $x_{LLW}$  and  $W$  are the Lea, Leask and Wolf parameters;<sup>24</sup> and  $\Delta E_{a-b}$  is the energy difference between ground state  $\Gamma_a$  and first excited state  $\Gamma_b$ .

$x$	$\rho(300\text{ K})$ ( $\mu\Omega\text{ cm}$ )	$\rho(0\text{ K})$ ( $\mu\Omega\text{ cm}$ )	RRR	%Sb	$x_{LLW}$	$W$	$\Delta E_{3-5}$ (K)	$x_{LLW}$	$W$	$\Delta E_{1-5}$ (K)	$\Delta E_{1-4}$ (K)
				$\Gamma_3$ ground state				$\Gamma_1$ g.s.			
0	155	1.67	93	25.0	-0.721	-5.69	10.1	0.500	1.99	5.87	—
0.05	235	18.7	13	15.1	-0.720	-6.38	12.1	0.484	1.47	7.08	—
0.1	259	46.0	5.6	21.3	-0.717	-7.05	15.9	0.462	1.31	9.54	—
0.15	215	27.0	8.0	15.6	-0.718	-7.00	14.9	0.452	1.11	9.43	—
0.2	510	54.0	9.4	27.3	-0.713	-6.16	16.6	—	—	—	—
0.3	—	—	—	8.0	-0.707	-7.48	25.5	—	—	—	—
0.4	343	58.2	5.9	20.2	-0.702	-6.43	25.2	—	—	—	—
0.5	—	—	—	4.9	-0.687	-6.06	34.2	—	—	—	—
0.6	305	67.4	4.5	6.6	-0.675	-5.75	40.3	—	—	—	—
0.7	166	34.8	4.8	10.1	-0.663	-4.81	40.4	—	—	—	—
0.75	—	—	—	17.2	-0.669	-5.54	42.8	—	—	—	—
0.85	—	—	—	6.3	-0.670	-6.05	46.4	-0.737	2.70	—	87.4
0.9	330	42.4	7.8	11.9	-0.646	-4.58	47.7	-0.872	3.43	—	78.8
0.95	—	—	—	20.8	-0.665	-5.94	48.8	-0.970	5.51	—	88.7
1	578	41.8	14	7.4	-0.946	-5.45	50.8	-0.946	4.95	—	88.1